ACS APPLIED MATERIALS & INTERFACES

www.acsami.org

Research Article

# Nanoscale Events on Cyanobiphenyl-Based Self-Assembled Droplets Triggered by Gas Analytes

Efthymia Ramou, Susana I. C. J. Palma, and Ana Cecília A. Roque*

Cite This: ACS Appl. Mater. Interfaces 2022, 14, 6261−6273

Read Online

ACCESS | Metrics & More | Article Recommendations | Supporting Information



**ABSTRACT:** Liquid crystals (LCs) are prime examples of dynamic supramolecular soft materials. Their autonomous self-assembly at the nanoscale level and the further nanoscale events that give rise to unique stimuli-responsive properties have been exploited for sensing purposes. One of the key features to employ LCs as sensing materials derives from the fine-tuning between stability and dynamics. This challenging task was addressed in this work by studying the effect of the alkyl chain length of cyanobiphenyl LCs on the molecular self-assembled compartments organized in the presence of ionic liquid molecules and gelatin. The resulting multicompartment nematic and smectic gels were further used as volatile organic compound chemical sensors. The LC structures undergo a dynamic sequence of phase transitions, depending on the nature of the LC component, yielding a variety of optical signals, which serve as optical fingerprints. In particular, the materials incorporating smectic compartments resulted in unexpected and rich optical textures that have not been reported previously. Their sensing capability was tested in an in-house-assembled electronic nose and further assessed via signal collection and machine-learning algorithms based on support vector machines, which classified 12 different gas analytes with high accuracy scores. Our work expands the knowledge on controlling LC self-assembly to yield fast and autonomous accurate chemical-sensing systems based on the combination of complex nanoscale sensing events with artificial intelligence tools.

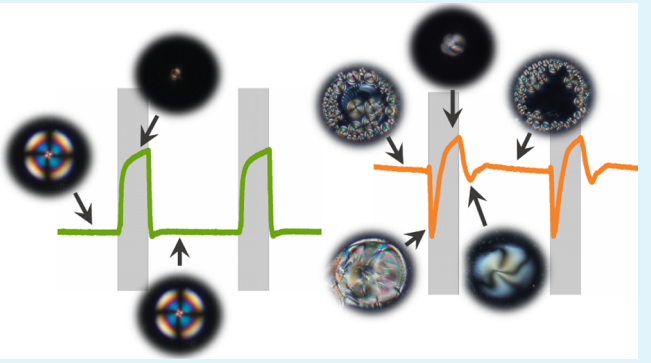

**KEYWORDS:** *nanoscale, liquid crystal, ionic liquid, self-assembly, electronic nose, machine learning*

## INTRODUCTION

Soft matter is an enticing approach toward designing functional chemoresponsive materials due to their tuneable self-assembly and dynamic properties occurring at the nanoscale level.[1] In this respect, liquid crystals (LCs) represent a great example of dynamic structure formation and reformation via self-assembly.

LCs are considered ordered fluids. They flow like conventional liquids but also exhibit significant orientational order and, in some cases, positional order. Liquid crystalline materials respond to perturbations occurring in their molecular organization resulting from external stimuli such as electrical or magnetic fields, surface effects, mechanical shear, temperature, and chemical analytes.

Sensing targeted chemical species is an ongoing trend application of LCs since they can act as optical probes with low power consumption, operation at room temperature with simple instrumentation, and with excellent opportunities for high selectivity at the molecular level. As a result, gas and volatile organic compound (VOC) sensors incorporating an LC element are gaining increasing interest and have so far demonstrated their potential as promising alternatives to conventional gas-sensing platforms.[2] In general, this capability arises from the fact that gas and VOC molecules can diffuse into the LC surface, resulting in a change of the liquid crystalline molecular orientation[3−5] or a decrease of the order parameter,[6−9] depending on the geometry of the system.

Typical sensor formats are LC films with a free surface,[10,11] spherical droplets,[12,13] and fibers.[14,15] A great majority of these studies employ thermotropic nematic LCs; however, a variety of LC phases exist, such as the smectic A phase. On the other hand, spherical geometries are considered an effective platform among LC-based sensing formats due to the large surface-area-to-volume ratio facilitating increased sensitivity. Recently, LC−ionic liquid (IL) droplets embedded in a biopolymeric matrix emerged as gel-like materials for VOC sensing. Exposing these hybrid gels to VOCs resulted in a decrease of the order parameter of the LC molecules inside the droplets, which in certain cases triggered a phase transition.[6,7] The LC used was the nematic 5CB (4-cyano-4′-pentylbiphenyl). Considering

Received: December 21, 2021
Accepted: January 10, 2022
Published: January 19, 2022

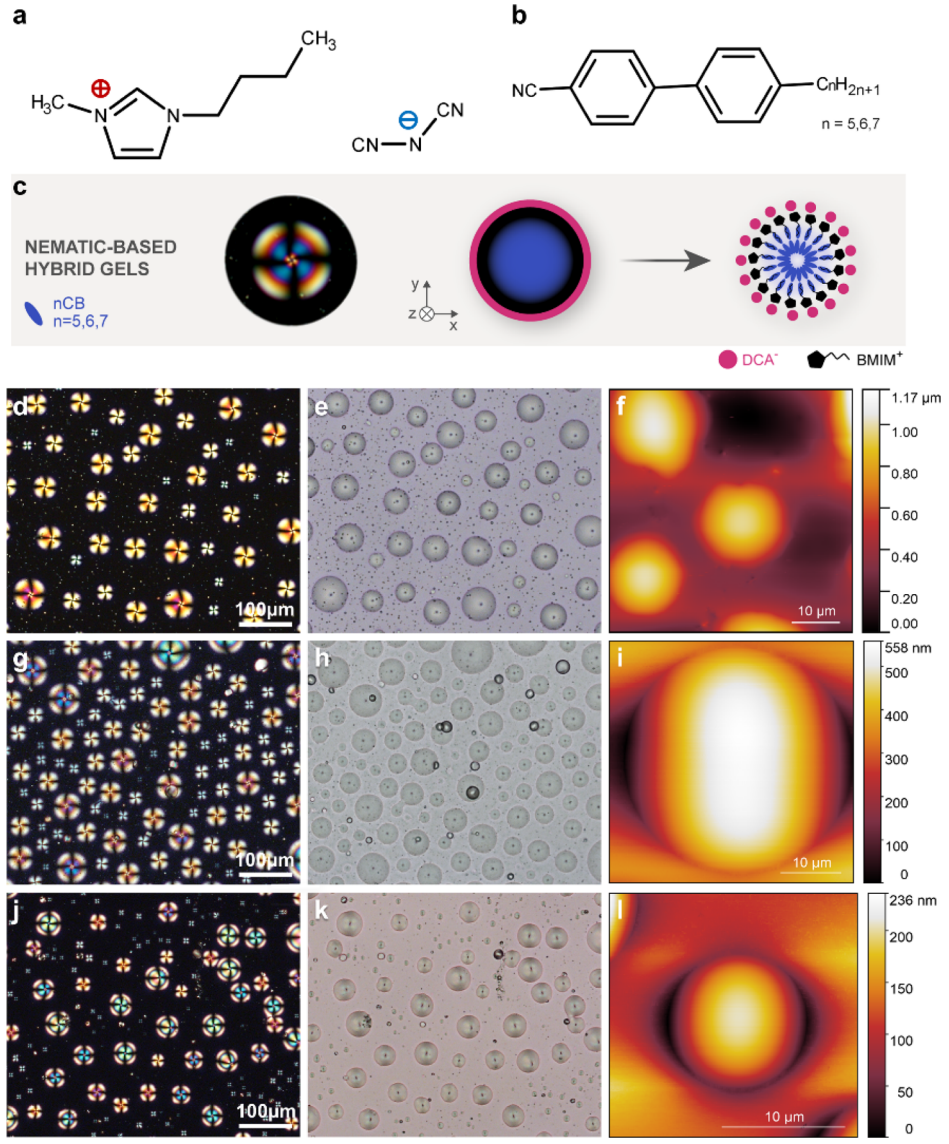


**Figure 1.** Optical, thermal, and morphological characterization of the nematic-based hybrid gels containing gelatin, [BMIM][DCA], and a nematic LC component. (a) IL [BMIM][DCA], (b) nematogenic members of the homologous series of alkyl-cyanobiphenyl LCs, (c) microscopy photograph of a nematogenic droplet with a radial director profile and schematic illustration of the IL−LC droplets, (d,g,j) polarizing optical microscopy micrographs with crossed polarizers, (e,h,k) corresponding bright-field micrographs, (f,i,l) AFM images, (d−f) hybrid gel containing gelatin, [BMIM][DCA], and 5CB, (g−i) hybrid gel containing gelatin, [BMIM][DCA], and 6CB, and (j−l) hybrid gel containing gelatin, [BMIM][DCA], and 7CB.

that VOC molecular recognition and selectivity result from the dynamic nanoscale assembly of the gel components, such as the LC moiety, a question remained to be studied on the effect of the LC structure on the reversible self-molecular organization of LC droplets.

The current study is focused on answering this question (i) by revealing for the first time the molecular self-organization of room-temperature nematic and smectic LCs of the cyanobiphenyl family of nCBs and (ii) by using the gel formulations as gas-sensing elements in a custom-made prototype electronic nose (e-nose) tailored to monitor light transmittance. Interestingly, hybrid gels containing 8CB, which exhibits the smectic A phase, self-assembled into molecular systems that yielded rich optical textures and optical signal profiles upon sequential VOC exposure to 12 distinct analytes (heptane, hexane, toluene, chloroform, dichloromethane, diethyl ether, ethyl acetate, acetone, acetonitrile, ethanol, methanol, and acetic acid). The signals were further analyzed using a uniquely developed machine learning algorithm based on support vector machines (SVM) for the classification of the tested volatiles. The best overall performance was exhibited by the 5CB and the 8CB hybrid gel compositions (evaluated via the correct predictions of the algorithm). As such, our results expand the hidden potential of LCs as nanoscale tools for chemical sensing.

## RESULTS AND DISCUSSION

### Morphological Characterization of nCB Hybrid Gels.

It is already known that 5CB can be encapsulated in [BMIM][DCA] spherical interfaces via cooperative assembly and furtherly stabilized within a biopolymeric matrix (gelatin),[6,7,16] overall forming a multicomponent gel. [BMIM][DCA] is a methylimidazolium-based IL, a class of compounds comprised entirely by ions. Here, dicyanamide ([DCA]$^-$) is



https://doi.org/10.1021/acsami.1c24721
ACS Appl. Mater. Interfaces 2022, 14, 6261−6273

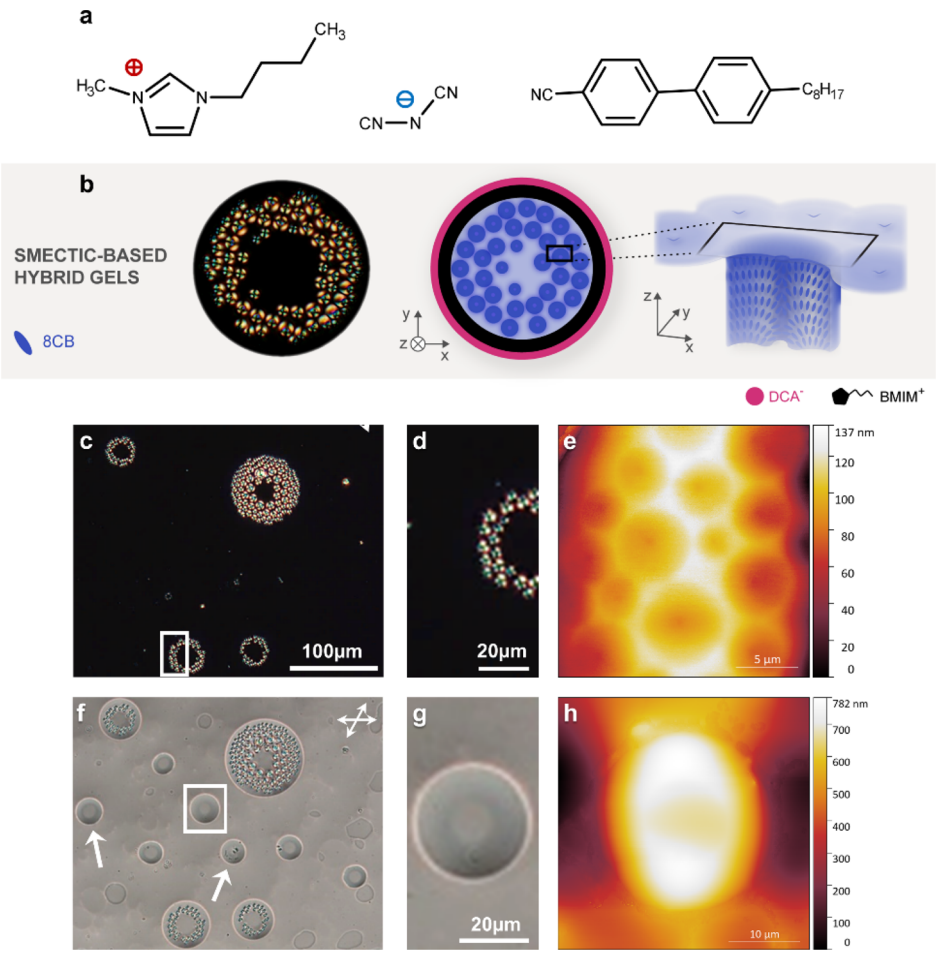


**Figure 2.** Optical and morphological characterization of the smectic-based hybrid gels containing gelatin, [BMIM][DCA], and 8CB. (a) IL [BMIM][DCA] and the smectogenic 8CB, (b) microscopy photograph of an 8CB droplet exhibiting a ring of TFCDs, which suggests that the projection of the director field onto the plane of the substrate is radial within the area contained in the circular basis of the defect,[21] (c) micrograph with crossed polarizers of a hybrid gel prepared with 8CB, (d) enlargement of the area depicted inside the white rectangle in (c), (e) AFM topographical image of the toric focal domains in a ring formation, (f) bright-field photograph of the texture shown in (c). The white arrows mark some of the IL interfaces that appear dark under crossed polarizers, for example (c), (g) enlargement of the area depicted inside the white rectangle in (f), and (h) AFM topographical image of one of the droplets that appear dark under crossed polarizers.

the anion. The gel formulation results in a physical compartmentalization of the constituents that gives rise to a unique stimuli-responsive material with electro-optical properties. The neat LCs studied here were four members of the homologous series of alkyl-cyanobiphenyls (nCBs) with a number of carbon atoms in the alkyl chain, ranging from five to eight (5CB−8CB), see Figures 1 and 2.

The first step of our investigations was the morphological characterization of the hybrid gels by polarized optical microscopy (POM) at room temperature, in order to study the shape, size, and population of the assembled droplets and the determination of the adopted director profiles within the droplets. It has been already reported by Hussain et al.[7] and Esteves et al.[6] that hybrid gels containing 5CB (Figure 1d,e) exhibit polydisperse droplets, featuring a radial configuration. The distinctive Maltese cross pattern, seen in POM under crossed polarizers, does not change upon rotation of the sample due to the spherical symmetry of the director profile.[17] Furthermore, in bright-field images (Figure 1e), the characteristic core defect, named hedgehog, located in the center of the droplet can be observed. The radial director configuration suggests that the LC molecules are aligned perpendicularly at the IL interface. This is probably achieved through molecular interactions generated between the alkyl moieties of [BMIM]-[DCA] and the 5CB mesogen, as previously reported.[6,7] Similar POM morphologies with radial polydispersed droplets were observed for the 6CB hybrid gel (seen in Figure 1g,h) and 7CB hybrid gel (seen in Figure 1j,k). The droplet diameters vary between 10 and 25 $\mu$m (see Figure S1 in the Supporting Information). On the other hand, the control gels without the IL exhibit LC droplets, some of them being irregularly shaped, with a bipolar or a random planar director configuration (see Figure S2 in the Supporting Information). This strengthens the importance of the IL regarding the shape of the assembled droplets and most importantly the anchoring and further orientation it can provide to the LC component.

Hybrid gels containing 8CB presented instead of radial droplets bright rings comprised by smectic defects (Figure 2). Their diameters are typically larger than the gel thickness (roughly 35 $\mu$m, see Figure S1 in the Supporting Information), indicating that they are deposited on the substrate and not in the bulk. Whereas all the LC compounds used for the preparation of the gels exhibit the nematic phase at room temperature, 8CB is smectic and the result is this unexpected


https://doi.org/10.1021/acsami.1c24721
ACS Appl. Mater. Interfaces 2022, 14, 6261−6273

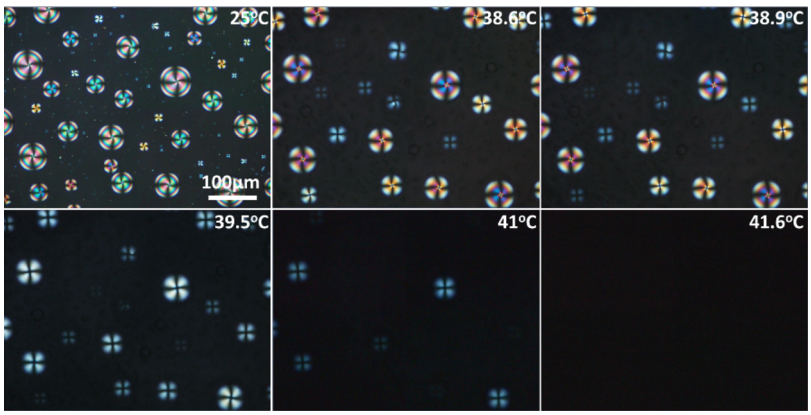


**Figure 3.** Polarized optical micrographs taken with crossed polarizers during heating from room temperature of a hybrid gel containing 7CB.

smectic texture. On the other hand, control 8CB gels, without [BMIM][DCA], present droplets which do not have a preferred director configuration and exhibit smectic-like defects (see Figure S2g,h in the Supporting Information).

Upon closer inspection of the deposited smectic rings, it became obvious that the defects are in fact toric focal conic defects (TFCDs) generated by layers folded around conjugated lines and circles as can be seen in the schematic in Figure 2b.[18−20] This texture typically stems from hybrid boundary conditions. In our case, since the IL interface promotes a homeotropic anchoring of the LC molecules, we suggest that the alignment changes gradually as we reach the bottom of the glass substrate. Probably, the spreading procedure promotes a more planar orientation at the bottom part of the droplet, resulting in an overall hybrid alignment. Another interesting detail revealed by investigations of 8CB hybrid gel textures taken in bright-field microscopy conditions was the existence of several IL interfaces (see Figure 2f, some of them are marked with a white arrow) where the orientation of 8CB lies along the observation axis, which is perpendicular to the substrate and perpendicular to the IL interface at the top of the droplet surface, making them appear dark under crossed polarizers (from now on, we will refer to those interfaces as dark droplets).

The morphology of the gels was further investigated through AFM. Hybrid gel compositions prepared with 5CB, 6CB, and 7CB exhibit smooth surfaces and the IL−LC droplets that assemble are symmetrical and smooth protuberances, with heights between 0.2 and 1 $\mu$m (see Figure 1f,i,l respectively). The plots in Figure S3 represent a cross section of their corresponding AFM morphology photographs along two directions and help visualize better the droplet profiles.

Contrary to the AFM results of the nematic-based hybrid gels, the TFCDs exhibited by the 8CB hybrid gels present a totally different topography. The patterns generated by AFM investigations are associated with depressions on the surface of the gel (see Figure 2e), a typical characteristic for TFCDs.[22] According to the cross section plot (Figure S4), these depressions are symmetrical, a finding that also confirms that the smectic defects forming the rings seen under crossed polarizers in POM are indeed TFCDs. Depending on their size, the depth of the depressions can vary from 0.02 up to 0.1 $\mu$m.

Another interesting observation, revealed by AFM studies, was that the interfaces that encapsulate 8CB may be symmetrical with a smooth surface, but the central part is bent toward the glass substrate (see the dark droplet in Figures 2h and S4 for cross section plots and a droplet with ring formation). Revisiting the POM photograph with uncrossed polarizers in Figure 2, we note that the central parts of both the ring-forming and the dark droplets (the latter marked with a white arrow) have a different color than in their periphery, which can be associated with the bent profile revealed by AFM observations. It can be hypothesized that the bending occurs as a result of the packing of IL headgroups coupled with the smectic nature of 8CB,[23,24] facilitating altogether the ring formation of TFCDs.

We also performed AFM investigations in control gels prepared without [BMIM][DCA] (see Figure S5 in the Supporting Information). These gels present rough surfaces with droplets that can be either protuberances or holes. Cross section plots of the acquired AFM topography photos reveal that the assembled LC droplets do not exhibit symmetrical profiles, similar to the results reported by Hussain et al.[7] for control gels containing 5CB.

The diameter size distribution of the assembled droplets in all the hybrid gels was also studied (Figure S1 in the Supporting Information). Interestingly enough, the distributions depend on the LC present in the hybrid formulations. More specifically, from Figure S1, we can deduce that the droplet diameters vary as the aliphatic terminal chain of the LC increases. It is also observed that for gels containing 5CB (Figure S1a) and 7CB (Figure S1c), the distribution of the diameters is quite narrow, with a dominant value around 10−15 $\mu$m for 5CB[6] and 15−20 $\mu$m for 7CB. In the case of 7CB, the distribution extends to higher values, but with low counts. On the other hand, 6CB (Figure S1b) and 8CB (Figure S1d) exhibit wider distributions with a variety of diameter values, which are non-negligible. This could be attributed to the parity of the alkyl chain of the LCs. It could be another interesting manifestation of the well-known odd−even effect first observed in LC dimers,[25,26] but it also characterizes the monomers of the nCB homologous series, where material properties are dependent on the number of carbon atoms in the alkyl chain.[27−29]

Lastly, the morphological characterization investigations of the hybrid gels were concluded by studying the droplet stability during storage over a 30-day period. The resulting representations of the relative variation of the droplets' position and size over time can be found in the Supporting Information (Figures S6−S9). With the exception of the 7CB-based hybrid gel, the rest of the LC-containing gel


https://doi.org/10.1021/acsami.1c24721
ACS Appl. Mater. Interfaces 2022, 14, 6261−6273

compositions exhibited fairly stable droplets at room storage conditions, with no substantial variations in their size or position. On the other hand, the results for the 7CB gels revealed that humidity variations during storage affected the droplet morphology greatly, that is, droplet translation leading to coalescence into larger inclusions or IL interfaces tearing and generating LC spillage into the matrix, to name a few.

**Thermal Characterization of nCB Hybrid Gels.** Detailed thermal studies via POM using a heating/cooling hotstage were performed on all the hybrid and control gels. With regard to the nematic-based gels, an example is depicted in Figure 3 where a 7CB hybrid gel is heated from room temperature during POM observation at a 3 °C $min^{-1}$ temperature rate. At 37.9 °C, the nematic−isotropic transition starts, observed first for the smaller droplets (see, e.g., at 38.6 °C in Figure 3). As the temperature increases, the larger droplets follow, and isotropization is concluded at 41.6 °C (at a temperature slightly below that of the isotropization of the neat 7CB compound, observed at 42.1 °C via POM). Evidently, the size and shape of the LC droplets confined in spherical cavities influence the transition temperatures.[30,31] In the case of control gels (see Figure S10) and during heating from room temperature, isotropization starts from the large droplets followed by the smaller droplets, a process carried out over several degrees of temperature. This is comparable with what has been observed for polymer-dispersed LCs prepared by phase separation, where a small fraction of mesogen remains in the polymer matrix.[32] Phase transition temperatures were also assessed using differential scanning calorimetry (DSC) and are featured in Table 1. The neat LC compounds are also included for comparison purposes.

**Table 1. Transition Temperatures for the Nematic-Based Gels and Neat Compounds**[a]

| | | Cr → N (°C)[+] | N → Iso (°C)[+] |
|---|---|---|---|
| 5CB | neat | | 33.3 |
| | hydrogel | | |
| | hybrid gel | | 32.7 |
| 6CB | neat | 13.0 | 25.6 |
| | hydrogel | | |
| | hybrid gel | 14.8 | 26.8 |
| 7CB | neat | 17.3 | 40.9 |
| | hydrogel | | |
| | hybrid gel | 15.8 | 39.6 |

[a]The temperatures were taken from the second DSC heating scan. [+]Cr = crystal; N = nematic; Iso = isotropic.

Studies of the textural transformations of the 8CB hybrid gels upon varying the system's temperature were performed on both the ring arrangements of the TFCDs and on the dark droplets. Specifically, we quickly heated the hybrid gel until 8CB was isotropic (approximately at 41 °C) and let the gel remain at that temperature for 5 min. We subsequently began to cool down the sample with a temperature rate of 3 °C $min^{-1}$ while observing through the POM.

In the case of the TFCD rings (Figure 4a), the isotropic to nematic transition was detected at 38.9 °C. In the nematic phase, the 8CB droplets feature a radial configuration. The transition to the smectic A phase occurred at 32.2 °C and was marked by the appearance of a striped texture. The stripes develop along the nematic director field, originating from the periphery of the droplet. However, as it has been reported for several smectic systems with hybrid boundary conditions, the striped texture is not stable.[33,34] The stripes quickly transform into toric focal conic domains via an intermediate corrugated texture named virgule. Upon further cooling, dark areas start appearing around the center of the droplet, for example, as seen in Figure 4a at 29.7 °C, finally resulting in a ring arrangement of the toric focal conics at room temperature. This could be attributed to an induced homeotropic alignment due to the adsorption of the IL aliphatic tails into the LC to a certain extent. In the Supporting Information in Figure S11, a similar series of photos can be found, obtained without the analyzer. Thus, it is easy to identify the existence of the hedgehog defect in the nematic phase of 8CB and realize that during the nematic to smectic transition, the adsorption of [BMIM][DCA] into 8CB does not occur only at the center of the droplet but also in the periphery of the interface.

The textural transformations upon cooling of the dark droplets can be seen in Figure 4b. The isotropic to nematic transition occurred at 38.7 °C, whereas the nematic to smectic A transition started at 32.4 °C. The patterns developing during the transition are identical to those seen in Figure 4a, with stripes as the initial texture followed by the formation of TFCDs. However, in this instance, the appearance of the dark patches does not stop at the periphery of the interface but continues to completion, creating a completely pseudo-isotropic texture, for example, at 30.9 and 25 °C in Figure 4b. In Table 2, the phase transition temperatures of the smectic-based gels and neat compound can be found, extracted from DSC scans. The DSC thermograms for all the studied nematic- and smectic-based gels can be found in Figure S12. Additionally, ATR−FTIR spectra of all the studied gel formulations and controls (e.g., gelatin hydrogel, pure [BMIM][DCA], and neat LC compounds) are shown in Figure S13, which suggest that the presence of the LC component does not affect the overall gel organization established in the final hybrid formulation. This is corroborated by Raman spectroscopy investigations, seen in Figure S14, depicting a compartmentalization of the LC droplets within the gelatin−IL matrix.

**Hybrid Gel Optical Properties upon VOC Exposure.** Our approach relies on the notion that VOC molecules diffusing into a LC surface can result in a decrease of the order parameter, potentially leading to an analyte-induced phase transition.[3−9] For control purposes, we first tested spin-coated films of the studied pure LCs under the presence of various gas analytes at room temperature and confirmed via POM that the tested diffusants could prompt a shift in the LC transition temperatures toward lower values[14] (see the Supporting Information for more details in Figures S15 and S16).

The textural transformations of hybrid gels containing 5CB upon exposure to VOCs have been already reported by Hussain et al.[7] and Esteves et al.[6] According to their POM observations, analyte molecules diffuse into the self-assembled droplets and decrease the organization of the LC mesogens. In most cases, this triggers a nematic to isotropic transition, which is reversible when the gas analyte is flushed out of the system with ambient air. In this work, the optical investigation of the nCB hybrid compositions in the presence of gas analytes was conducted with the use of an in-house-designed glass chamber placed between the crossed polarizers of the POM (see the Methods section for details). During each experiment, images and videos were recorded for further analysis. The hybrid gels containing the nematic LC compounds studied here exhibit


https://doi.org/10.1021/acsami.1c24721
ACS Appl. Mater. Interfaces 2022, 14, 6261−6273

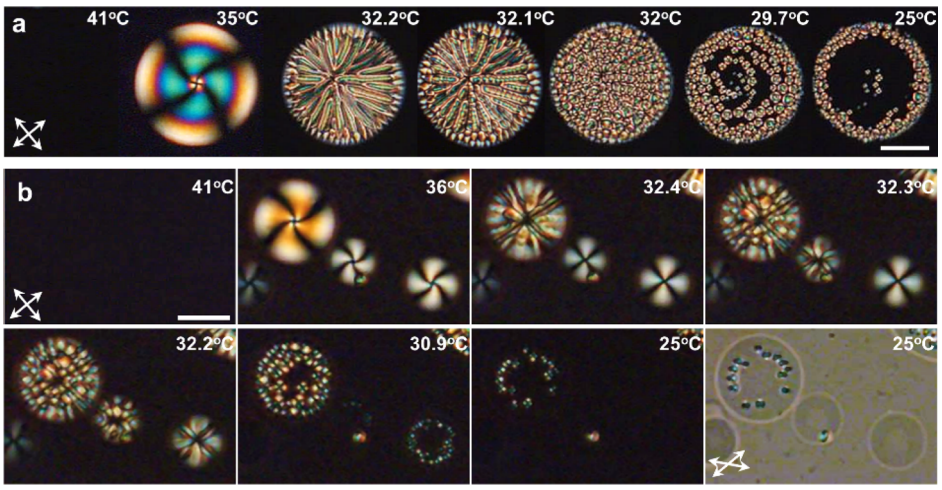


**Figure 4.** POM micrographs of 8CB droplets assembled in hybrid gels. The photographs are taken upon cooling from the isotropic state, (a) droplets forming TFCDs in ring formations, (b) dark droplets. The white line corresponds to 50 $\mu$m.

**Table 2. Transition Temperatures for the Smectic-Based Gels and the Neat Compound**[a]

| | | Cr → SmA (°C)$^+$ | Cr → N (°C)$^+$ | SmA → N (°C) | N → Iso (°C)$^+$ |
|---|---|---|---|---|---|
| 8CB | neat | 19.3 | | 30.7 | 37.9 |
| | hydrogel | | | | |
| | hybrid gel | | 15.0 | | 38.3 |

[a]The temperatures were taken from the second DSC heating scan. The smectic A to nematic transition was not traced by the DSC for the 8CB hydrogel and the 8CB hybrid gel. $^+$Cr = crystal; SmA = smectic A; N = nematic; Iso = isotropic.

pattern changes, when responding to the 12 gas analytes, similar to the previously reported gel composition.[6,7]

An example is given in Figure 5a, where a 5CB hybrid gel is exposed to hexane vapors for a single cycle. During exposure, the nematic droplets start shrinking until the whole field of view is dark. It is interesting to note that the smaller droplets disappear first, followed by the larger ones, on par with the thermal investigations. Upon the recovery period, the reverse was observed. Moreover, it is evident that the isotropic−nematic transition starts from the periphery of the droplet because this is where the gas is expelled from. This whole process has proven to be repeatable, on par with the pure LC experiments (see the Supporting Information).

Regarding POM studies of 8CB hybrid gels, the textural changes during the experiments are more complex, when compared to nematic-based gels. For example, in Figure 5b, the response of an 8CB hybrid gel to vapors of ethyl acetate is depicted for a single cycle. This experiment involves the observation of the ring formations of toric focal conic domains. Upon exposure to ethyl acetate, the diffusion of the analyte inside the IL interface decreased the LC order, and the exposure duration was enough to trigger a smectic A to a nematic and finally an isotropic transition within 3.9 s. These transitions start from the periphery of the droplet (e.g., seen in Figure 5b at 0.7 s) as it is the entering point for the diffusant. When the recovery period started, the reverse process was detected. The isotropic−nematic transition began from the periphery of the IL interface (5.1 s in Figure 5b), similar to the 5CB hybrid gel case. Upon completion of the nematic transition, a radial-like configuration was observed (6.3 s in Figure 5b). This was followed by the nematic−smectic A transition, presenting a stripe-like pattern superimposed onto the previous nematic texture, as seen at 7.3 s in Figure 5b. The transformation was completed with the formation of the ring configuration of TFCDs.

The response of dark droplets formed in 8CB hybrid gels in the presence of gas analytes, as observed through the POM, is worth mentioning. As an example, exposure to chloroform vapors is depicted in Figure 5c. On par with the previously discussed experiment, the diffusion of chloroform inside the dark droplets prompts a smectic A to nematic (0−0.6 s in Figure 5c) to isotropic transition, which in this experiment was completed within 3.2 s. In the recovery period, following a well-defined isotropic to nematic transition (6.3−6.9 s Figure 5c), the transition to the smectic A phase is less defined (8.3−14.8 s in Figure 5c). It manifests as a dark texture starting from the periphery of the droplet and advances toward the center, while the nematic phase continues to develop. After further time, the nematic texture shrinks and disappears, leaving the smectic phase to fully develop into a pseudo-isotropic texture. This contraction of the nematic texture is possibly due to adsorption of the [BMIM][DCA] within the 8CB, promoting a homeotropic orientation[23] in conjunction with the bending of the central part of the interface. It should be noted that an apparent shrinking of textures occurs in the toric focal conic ring-type droplets as well, but it is not always prominent. For example, in Figure 5b, it became more obvious during the transition to the smectic A phase (6.3−7.3 s in Figure 5b), but the development of the TFCDs within the ring negates the effect. This may be due to the dynamic state of molecular rearrangement within the droplet, correlated with the fast absorption/desorption rate of the diffusant, which results in such rich textural changes.

As for the performance of the control gels, without [BMIM][DCA] in the presence of gas analytes as observed via POM, an example is shown in Figure S17 of an 8CB control gel, where the composition is exposed to acetone for a single cycle. The presence of the acetone vapors led to a decrease in the order parameter, driving the majority of the droplets to isotropization. Almost identical to the thermal investigations on control gels, the larger droplets turned isotropic first and the smaller ones followed. Upon recovery,


https://doi.org/10.1021/acsami.1c24721
ACS Appl. Mater. Interfaces 2022, 14, 6261−6273

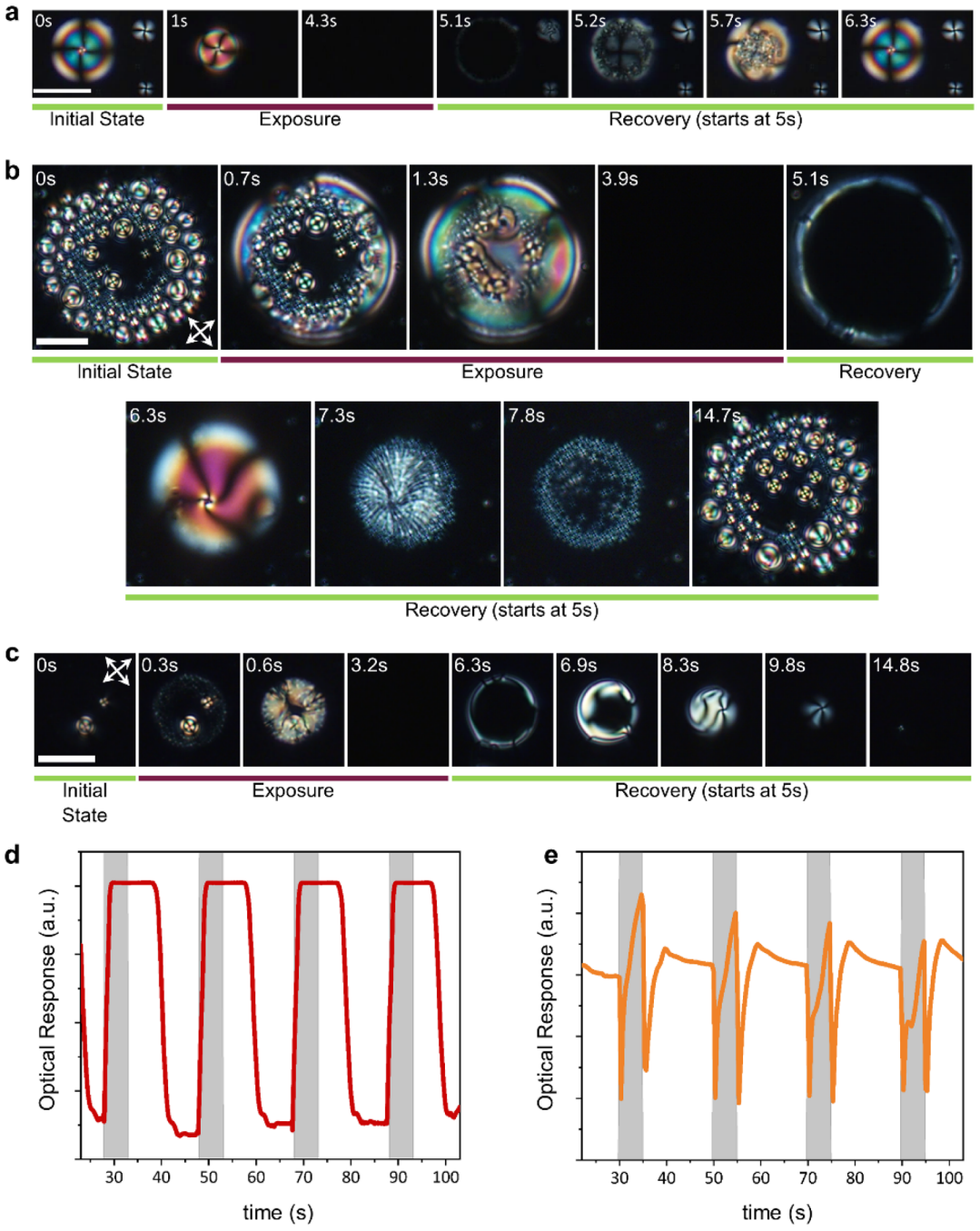


**Figure 5.** Textural changes of hybrid gels during exposure to vapors of (a) hexane, (b) ethyl acetate, and (c) chloroform and subsequent recovery, as observed through the POM and corresponding signals extracted from video analysis. POM photos were taken with crossed polarizers at room temperature, (a) 5CB hybrid gel. The hexane vapors drive 5CB to isotropization, whereas during the recovery period, the nematic radial droplets are restored. Time stamps refer to the time after the start of exposure. The white line corresponds to 50 $\mu$m, (b) ring formation of TFCDs exhibited by a hybrid gel containing 8CB. 0 s: initial state, exposure to ethyl acetate starts, 0.7 s: onset of the smectic A to nematic transition, 1.3 s: nematic phase almost at completion, 3.9 s: 8CB turns isotropic. At 5 s, diethyl ether is expelled and the recovery period starts. 5.1 s: isotropic to nematic transition, 6.3 s: nematic phase, 7.3 s: onset of the nematic to smectic A transition, 7.8 s: onset of the TFCD formation, 14.7 s: completion of the TFCD formation. The white line corresponds to 25 $\mu$m. Time stamps refer to the time after the start of exposure, (c) dark droplets formed in 8CB hybrid gels. 0 s: initial state, exposure to chloroform starts, 0.3 s: onset of the smectic A to nematic transition, 0.6 s: progress of the nematic phase formation, 3.2 s: 8CB turns isotropic. At 5 s, chloroform is expelled and the recovery period starts, 6.3 s: isotropic to nematic transition, 6.9−9.8 s: nematic phase progress toward the smectic A transition, 14.8 s: smectic A phase. The white line corresponds to 50 $\mu$m. Time stamps refer to the time after the start of exposure. An example of the signals was obtained through video frame analysis using ImageJ from e-nose experiments conducted using the polarizing optical microscope. Exposure to acetone vapors (calculated via ImageJ) is portrayed for the hybrid nCB gels (d) 5CB, (e) 8CB. Four consecutive cycles are depicted, each 5 s of exposure (gray columns) followed by 15 s of recovery with ambient air.

the reverse process was observed, and the smectic phase was fully restored in the gel.

The videos recorded during these POM experiments were analyzed with the use of the ImageJ software. Through frame



https://doi.org/10.1021/acsami.1c24721
ACS Appl. Mater. Interfaces 2022, 14, 6261−6273

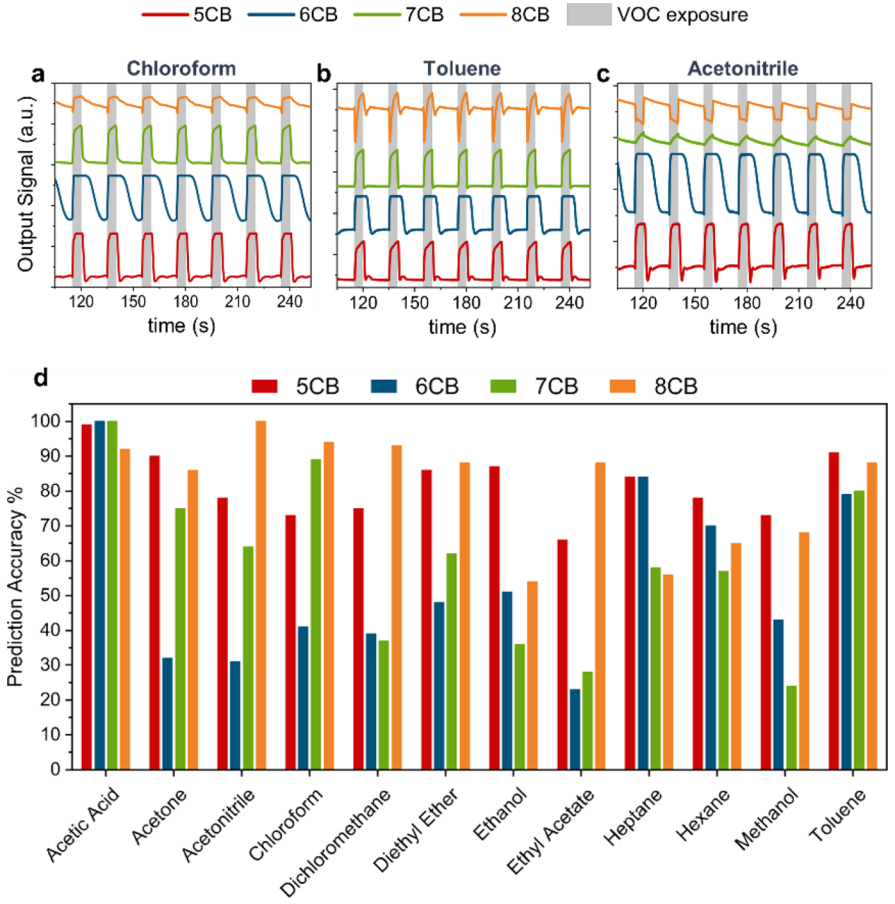


**Figure 6.** Example of the signals generated by the nCB-based hybrid gels during exposure to volatile vapors and a collective accuracy prediction plot for the 12 VOCs yielded by all the tested hybrid gels, (a) exposure to chloroform, (b) exposure to toluene, and (c) exposure to acetonitrile. Seven cycles are depicted here, each of 5 s of exposure (gray columns) and 15 s of recovery with ambient air and (d) bars prediction plot represents the prediction accuracy of the automatic classifier trained and tested with the collected e-nose signals.

analysis, the variation of the light intensity transmitted through the gels along time was determined, and the results were plotted against time. Examples can be seen in Figure 5d for the case of a 5CB based hybrid gel and in Figure 5e for an 8CB hybrid gel, both of them exposed to acetone vapors for four consecutive cycles. This representation can offer a first estimation on how the gels could perform on the e-nose. In these plots, an increase in the optical response corresponds to a decrease in the light intensity seen from the microscope. The two gels exhibit very different response profiles. In the case of the 5CB hybrid gel (in Figure 5d), the gel responded rather quickly in the presence of acetone, and complete isotropization was achieved within 2 s of exposure. However, the recovery process was quite slow, as it started after 5.4 s within the recovery period with ambient air. On the other hand, the prolific optical profile exhibited by the 8CB-based hybrid gel can be correlated with the multiple phase transitions the LC component undergoes during exposure and recovery. More examples can be found in the Supporting Information, in Figure S18.

It is important to comment on the interactions between the tested VOCs and the hybrid gel compositions. Overall, the system's reaction to the presence of an analyte depends on the chemical nature of the specific diffusant. We have already reported[6,7] that hydrophobic non-polar analytes (e.g. hexane, heptane, and toluene) may interact directly with the LC and similar to the presence of an impurity, they reduce the LC order parameter and lower its clearing temperature (an example can be found in Video S1 in the Supporting Information for a 5CB hybrid gel being exposed to toluene). Polar and protic analytes (such as ethanol, methanol, and acetic acid) tend to interact preferably with the IL and gelatin through hydrogen bonding and less with the LC component. These interactions can disrupt the IL interfaces, which leads to a disturbance of the LC order and potential droplet mobility within the medium (as an example, Video S2 in the Supporting Information shows a 8CB hybrid gel exposed to ethanol). For analytes with intermediate polarity, hydrophobicity, and hydrogen bond tendency, we believe that their interaction is a combination of their degree of preference toward the different compartments of the hybrid gel composition. Hence, different analyte affinities toward distinct gel compartments can trigger different magnitudes of response and affect differently the response/recovery process and potential LC isotropization. This leads to a variety of responses, which ultimately can serve as "fingerprint" responses.[6] Essentially, the combination of functional components is far more superior than the individual constituents in the hybrid sensors.

It is likely that hexane (5CB hybrid gel in Figure 5a) and both ethyl acetate and chloroform (8CB hybrid formulation seen in Figure 5b,c) interact preferentially with the LC component. Complete isotropization was achieved faster for ethyl acetate vapors (within 3.2 s) interacting with the 8CB hybrid composition. This signifies that among the presented


https://doi.org/10.1021/acsami.1c24721
ACS Appl. Mater. Interfaces 2022, 14, 6261−6273

LC compounds, this diffusant exhibits a higher affinity toward 8CB than, for example, for chloroform, even though we need to add that isotropization depends to a certain degree on the droplet size since analyte-induced transitions share characteristics with the thermally induced transitions. Furthermore, the rather slow recuperation of the texture depends probably on the geometry of the system and the restrictions it can impose on its components. Understandably, the pure neat LCs are faster (e.g., as seen in Figure S15 and S16), but as we mentioned earlier, the overall system of hybrid gels is superior to the neat components in terms of the overall performance toward gas analytes.

**Hybrid Gels as Sensors in the e-nose.** Our POM studies established that all the tested nCB hybrid gels can be utilized as sensors in a tailor-made e-nose device. During the e-nose experiments, the sensors were exposed sequentially to vapors of 12 different VOCs, which are representative of distinct groups such as alcohols, ketones, aliphatic, aromatic, and halogenated compounds. The sensors are exposed to vapors for 5 s, followed by a 15 s recovery period with ambient air (defined as a cycle). Typically, the experiment for one gas analyte lasts 7.5 min (22 cycles). The collected signals were plotted against time for each tested analyte for further assessment. As we mentioned earlier, the signals generated by all the sensors are the result of the collaborative performance of the individual components.

Figure 6 shows examples of the signals generated by the tested cyanobiphenyl-based gels when exposed to chloroform (Figure 6a), toluene (Figure 6b), and acetonitrile (Figure 6c). These signals are essentially the output voltage of the photodiode that monitors the light exiting the system. As the sample's brightness decreases (decrease of the LC order parameter/emerging isotropization), the signal amplitude increases. According to the plots, 5CB, 6CB, and 7CB hybrid gels yield upward signal profiles during exposure to gas analytes, which has proven to be typical for nematic droplets.[6,7,35] The profiles exhibit various differences in their features, for example, response/recovery profiles, response/recovery times, signal plateau during exposure, and signal amplitude. For example, both 5CB and 6CB signals reached a plateau during exposure in the depicted plots (i.e. isotropization was complete before the exposure period ended), whereas this was not the case for the 7CB signals, indicating that isotropization was not fully complete in all the nematic droplets of the sensor. 8CB signals exhibit richer profiles when compared to the nematic hybrid gels. The response to acetonitrile (Figure 6c) yields a downward signal, which indicates that the sample becomes brighter. According to POM studies, this occurs when analyte vapors enable a smectic A to nematic transition, but they are not sufficient enough to drive the LC to isotropization. When the gas analyte is able to fully disorganize 8CB, triggering a smectic A to nematic to isotropic transition, the variations in the light intensity transmitted by the sample can produce signals with such detailed profiles, like in the case of chloroform (Figure 6a) and toluene (Figure 6b).

With regards to analyte-induced isotropization, apart from the preferred affinity of a volatile, a secondary factor that could be considered is a potential threshold correlation between the LC clearing temperature and the VOC concentration needed to trigger a transition.[36] The higher the clearing temperature is, the more analyte amount is needed to induce a transition to the isotropic state. Noting that during our e-nose experiment, the analyte concentration is constant as the sample volume is fixed at 15 mL, this could be relevant in our work especially for the volatiles that interact directly with the LC component. This element could be responsible for the full isotropization tendency of 5CB- and 6CB-based hybrid gels in the case of chloroform, for example, but not for 7CB and 8CB hybrid gels (see Figure 6a for the corresponding signals and Table1 for transition temperatures).

Taking into consideration all these remarks, it is noteworthy to discuss the rather slow recovery profiles of the 6CB hybrid composition, seen in Figure 6. In some cases, the signal could barely reach the baseline before the next exposure, when compared to 5CB and 7CB, suggesting that a 15 s recovery period is insufficient for this LC compound. We opted to investigate further into this matter, performing e-nose experiments where 6CB hybrid gels were exposed to vapors of 12 analytes for 5 s with a 25 s subsequent recovery with ambient air, for 22 consecutive cycles per VOC. It was discovered that a longer recovery period facilitated efficiently the reorganization of 6CB nematic droplets, when recuperating from the isotropic phase. This resulted in the acquisition of well-rounded, fully featured signals, which aided in a better performance evaluation of this gel formulation (see details below). As an example of the collected signals, in Figure S19 in the Supporting Information, the response of 6CB hybrid gels to acetonitrile vapors with a recovery period of 25 s (Figure S19b) is shown. Signals acquired with a 15 s recovery period (Figure S19a) have been included for comparison purposes. We need to point out, however, that even with an extended recovery period, 6CB droplets are still rather slow in their recuperation from the isotropic phase, indicating that this could be an intrinsic property of 6CB toward the tested gas analytes. It is plausible that this is because 6CB has the lowest clearing temperature among the tested nCB LCs, meaning that a less amount of analyte would be needed to trigger an isotropic transition.[36] The excess amount of analyte vapors could result in an exaggerated suppression of the clearing temperature (impurity effect), leading to a slow recovery process when the VOC is flushed out of the system. This is a very interesting response behavior, and we intend to investigate more on this subject in our future works.

Control gel formulations were also tested in the e-nose for the whole spectrum of 12 volatile gases, for comparison purposes. Examples of the collected signals are presented in Figure S20 for the case of exposure to vapors of chloroform (Figure S20a), toluene (Figure S20b), and acetonitrile (Figure S20c). As seen in the plots, all the control formulations (including the 8CB-based gel) generate signals with an upward profile. It is interesting to note that the signal profiles still exhibit distinct differences in features such as response/recovery profiles, response/recovery times, and signal plateau during exposure or signal amplitude, although these gel compositions lack [BMIM][DCA]. An interesting detail is the spike-like signals generated by the 7CB- and 8CB-based control gels when exposed to acetonitrile (Figure S20c). This indicates for the case of the 7CB control composition that the acetonitrile vapors can indeed cause a disruption in the molecular organization; however, they cannot sustain it, thus allowing 7CB to recuperate back to its initial state during the exposure period (i.e., the signal reaches the baseline during exposure). Similarly, for the 8CB control gel, the acetonitrile vapors trigger a quick disorganization possibly to isotropization (i.e., the spike part of the signal profile); however, this is followed by an immediate downward curve, lower than the


https://doi.org/10.1021/acsami.1c24721
ACS Appl. Mater. Interfaces 2022, 14, 6261−6273

corresponding baseline, which suggests that the sample becomes brighter than when in its initial state, that is, 8CB recuperated quickly from isotropization and then transitioned to the nematic phase. Another notable observation is that in the case of the 6CB-based control formulation, a 15 s recovery period is quite sufficient for the LC to recuperate from isotropization, unlike the corresponding hybrid composition. At this point, we could hypothesize that in the control formulations, the gelatin matrix creates a rather rigid and stiff environment for the LC, whereas in the hybrid gels, the presence of the IL component results in a rather "mobile" interface, accommodating the fluidity of the LC while differently influencing the 6CB clearing temperature (see DSC thermograms for the liquid hydrogels in Figure S12). Profiles of all the signals collected for the whole spectrum of the 12 tested gas analytes can be found in the Supporting Information in Figure S21 (hybrid gels) and Figure S22 (control gels).

After signal collection, dedicated machine learning tools were employed in order to analyze our data. Signal features of two types, morphological features and parameters of curve fitting models,[6,37] were extracted and used as the input to train and test an automatic VOC classifier based on the SVM algorithm. Each gel formulation was analyzed independently from the rest. The classification results for each type of the studied LC-based hybrid gel are presented in a collective accuracy prediction plot, seen in Figure 6d. The bars represent the percentage of correct prediction for each VOC.

Overall, for the 5CB hybrid composition, the classifier exhibited high accuracy scores (above 70%) for all the tested VOCs, with the exception of ethyl acetate where the prediction was less accurate (between 57 and 64%). 6CB hybrid gels, tested with a 15 s recovery period, provided high accuracy predictions for acetic acid, heptane, hexane, and toluene, whereas the rest of the predictions were essentially random (below 50%). On the other hand, testing the 6CB hybrid gels with a 25 s recovery period increased the prediction performance of the sensor, as seen in Figure S23. The predictions of 7CB hybrid formulations were high for acetic acid, acetone, chloroform, and toluene, while the rest were a combination of less accurate and random predictions. Finally, for 8CB hybrid gels, the algorithm provided highly accurate predictions for most of the tested VOCs, with the predictions for ethanol, heptane, hexane, and methanol lying in the range between 54 and 68%. The complete classification performance of the SVM classifier is presented in confusion matrices for each hybrid composition, depicting the prediction results (both correct and incorrect) of the algorithm (see Figure S24 for the hybrid gels and Figure S25 for the 6CB hybrid gel tested with a 25 s recovery period). The overall accuracies of all the tested hybrid formulations (calculated from the average of the correct predictions), seen in Figure S26, demonstrate that the best gas-sensing performance was exhibited by the 5CB (81.7%) and 8CB hybrid gels (81%), while the 6CB hybrid sensor, when tested with a 15 s recovery period, performed the least (53.4%).

The overall performance of the control formulations is presented in Figure S20d. For the 5CB control gel, the algorithm exhibited a high accuracy for acetic acid, acetonitrile, and heptane, while the rest were a combination of less accurate and random predictions. In a similar vein, the classifier's performance for the 7CB and 8CB control formulations was rather poor for most of the tested gas analytes. Nevertheless, the predictions for the 6CB control composition were the most successful since highly accurate predictions were provided for acetic acid, dichloromethane, diethyl ether, methanol, and toluene. The overall accuracies for the control compositions are presented in Figure S25b, where clearly it is shown that the automatic classifier performed the best for the 6CB control gel (66.2%). Evidently, the predictions of the classifier were less successful, when compared to the hybrid formulations case, which irrevocably demonstrates that the hybrid LC gels are far superior in their gas-sensing performance. In the Supporting Information, confusion matrices for the control formulations can be found in Figure S27.

As a final note, we would like to comment on the outstanding potential of the automatic classifier since it allows the systematic processing and classification of the huge amount of signals collected during the e-nose experiments, a task that would be challenging for human researchers. As part of our future work, we intend to explore the possibility of the classifier's performance on a virtual array comprising the studied hybrid compositions and investigate their possible complementarity in terms of their VOC classification capabilities.

## CONCLUSIONS

The development of LC-based gas-sensing platforms is a fast-growing research field, opening a promising perspective for highly sensitive, fast, and low-cost chemical sensors. Confinement of LCs in spherical geometries can generate unique optical textures that serve as media for detecting molecular events at the nano-scale. Gas-sensitive LC-based gel compositions, which emerge from the cooperative assembly of functional components—LC−IL droplets, embedded in a biopolymeric matrix—were studied in this work for optical gas sensing, including nematic and smectic systems. The nematic-based sensors respond in a dynamic on/off manner, an alternation between the nematic and the isotropic state, in accordance with the current technological demands for materials with tuneable physical properties. On the other hand, the 8CB-based gels yield complex optical signals while undergoing successive transitions from the smectic A to the nematic to the isotropic states. The dynamic self-assembly features of the droplets and optical changes observed upon supramolecular (re)organization resulted in the acquisition of diverse optical signal profiles, which proved to be advantageous to efficiently discriminate and classify the tested gas analytes.

Without a doubt, the LC gel compositions exhibit essential sensing performance features such as sensitivity, selectivity, and fast response/recovery times. Most importantly, they present an elegant approach to the current challenges met by the conventional sensor formats, namely, cost of production, long-term stability, enhanced selectivity, and energy consumption. The gels are simple to prepare and store. They are versatile formulations and can be further functionalized with rationally chosen moieties for targeted sensing. The overall sensing platform uses simple and low-cost instrumentation, and the coupling with automatic pattern recognition tools has led to a system with improved performance, increased selectivity toward specific analytes, and operating at environmental conditions. Essentially, this work presents a systematic and creative approach toward real-time gas sensing and molecular recognition, by simply exploiting the cooperative assembly capabilities of soft materials.



https://doi.org/10.1021/acsami.1c24721
ACS Appl. Mater. Interfaces 2022, 14, 6261−6273

## METHODS

**Materials and Reagents.** The IL 1-butyl-3-methylimidazolium dicyanamide ([BMIM][DCA], >98%) was purchased from Iolitec. The LCs 4′-cyano-4-pentylbiphenyl (5CB), 4-heptyl-4′-cyanobiphenyl (7CB), and 4-cyano-4′-*n*-octylbiphenyl (8CB) were acquired from TCI Europe. 4-Cyano-4′-hexylbiphenyl (6CB) and gelatin from bovine skin (gel strength ≈225 g; Bloom, type B) were supplied by Sigma-Aldrich. Solvents used in the e-nose experiments: dichloromethane and hexane (purity ≥99.9%) were acquired from VWR, and ethanol (purity ≥99.8%) was purchased from Sigma-Aldrich. Acetonitrile (purity ≥99.9%), chloroform, diethyl ether (HPLC grade), ethyl acetate, heptane, methanol (HPLC grade), and toluene were supplied by Fisher Scientific. Acetone (purity ≥99.5%) was purchased from Honeywell. Milli-Q water was used. Solvents were of analytical grade and used as received.

**Hybrid Gel and Sensor Preparation.** All the gels in this work were produced following the protocol reported by Hussain et al.,[7] Semeano et al.,[16] and Esteves et al.[6] Optical gas sensors were prepared as follows: the gel formulation was deposited onto an untreated glass slide and spread into a film, using an automatic film applicator (TQC Sheen) equipped with a heated bed and a quadruplex with a predefined thickness of 30 $\mu$m. The films were left at room temperature for 24 h before being used either for characterization or an e-nose experiment. Control gel films were also made containing an LC component, gelatin, and water, for comparison purposes.

**Hybrid Gel Characterization.** All prepared gels (both hybrid and control gels) were initially characterized by POM using a Zeiss Axio Observer.Z1 microscope equipped with an Axiocam 503 color camera. Photographs taken were processed by the ZEN 203 software. The thermal behavior of the gels was investigated using a Zeiss Axioskop 40, equipped with a Linkam hotstage, an ECP water circulating pump for cooling, and an Axiocam 503 color camera. Photographs taken were processed by the ZEN 203 software. The diameter size distribution of the assembled droplets in the hybrid gels were determined using bright-field POM images of a sensor's active area. The diameters of the present droplets and their population on each photograph were defined using a python script. The results for each gel were presented in a histogram plot. AFM images were recorded using an Asylum Research MFP-3D Stand Alone AFM system operated in alternate contact (tapping) mode. The resulting topographs were plane-fitted. Further analysis of the photographs and cross-sectional plots were conducted using Gwyddion software. To observe the compartmentalization of LC droplets inside the gelatin−IL matrix, the surface of hybrid gel films was analyzed using Raman spectroscopy using a Witec Alpha 300 confocal RAS with a 532 nm argon laser at a 0.5 mW power. ATR−FTIR was performed using a PerkinElmer Spectrum Two FTIR spectrometer with a $LiTaO_3$/DTGS detector and an ATR accessory equipped with a ZnSe cell. Samples of hybrid gels, control hydrogels, and the neat LC compounds were prepared as described previously. Deuterium oxide was used instead of Milli-Q water during sample preparation. All measurements were made in the region between 400 and 4000 $cm^{-1}$ with 25 scans at room temperature and an atmosphere of ambient air. The background spectrum of ambient air was subtracted from the samples spectra and the results were presented in absorbance (%) units. Thermal investigations of the prepared gels (both hybrid and control gels) and neat LC compounds were conducted via DSC using a SETARAM DSC 131 calorimeter fitted with a liquid nitrogen cooling accessory. The equipment was calibrated before use against an indium standard. Two consecutive heating/cooling scans were performed, using scanning rates of 5 °C $min^{-1}$. Experimental data were taken from the second heating run.

In order to monitor the morphological changes of the assembled LC droplets in the hybrid gels upon storage at room conditions, we defined specific regions of interest on the hybrid gel films. We studied those regions through POM for 1 month, following any changes that could occur in the morphology. POM images with crossed polarizers were taken at 1 day and then 1, 2, 3, and 4 weeks after gel production. The resulting photographs were processed using a TrackEM2 plugin within Fiji (more details on the process can be found in Esteves et al.[6]). The resulting files were analyzed using a python script, which yields a representation of the relative variation of the position and size of the droplets with time.

**VOC Effect on Hybrid Gel Optical Properties.** For the visual observation of the VOC effect on the gels, the sensors (both hybrid and control gels) were placed in an in-house-designed glass chamber placed between the polarizers of an Axio Observer.Z1 microscope (details above). The gels were exposed to vapors of 12 different solvents (15 mL of the solvent preheated at 37 °C in a water bath for 15 min) for five consecutive cycles. Each cycle corresponds to a 5 s exposure to gas (via an air pump), followed by a 15 s recovery period with ambient air (via a second air pump), unless stated otherwise. During each VOC experiment, images and videos were recorded using the ZEN software. Frame analysis using the ImageJ software was performed on all the captured videos and the corresponding signal responses were determined by the variation of the intensity of the transmitted light through the gels along time. The results were plotted against time.

The prepared gels (both hybrid and control gels) were used as chemical sensors in the detection chamber of an in-house-assembled e-nose device.[6,35,37] The detection chamber, isolated from light and ambient air, includes six independent sensor slots. In each slot, a sensor is placed between crossed polarizers and paired with a light-emitting diode and a light-dependent resistor to monitor the light transmittance. The sensors are exposed sequentially to vapors of 12 solvents (15 mL of the solvent preheated at 37 °C in a water bath for 15 min) for 22 consecutive cycles. Each cycle corresponds to a 5 s exposure to gas, followed by a 15 s recovery period with ambient air, unless stated otherwise. The total solvent volume per analyte experiment was 15 mL. VOC concentrations have been measured indirectly via solvent evaporation.[6] The VOCs employed in all the e-nose experiments exhibit similar structures but belong to distinct groups, such as alcohol, ketones, aliphatic, aromatic, and halogenated compounds. Different batches of each tested gel formulation were produced, so that triplicates of each batch could be analyzed and ensure reproducibility of the results.

Processing of the acquired signals was performed using data analysis tools based on Python libraries (SciPy, scikit-learn, and novanistrumentation). A smoothing filter was first applied (20 points sliding window) and then a median filter, followed by dividing the signals into cycles and the subsequent normalization of each cycle. After that, the outliers were removed. Twelve features relevant to the morphology of the signal curves were extracted per cycle[37] and used as input to train an automatic classifier based on SVM. The classification results for all the gel compositions tested (both hybrid and control gels) were presented in normalized confusion matrices and accuracy plots.

The SVM classification model used in this work was implemented and optimized by our research group, as described in a previous publication,[37] using a data pool of signals generated by 5CB hybrid gels upon exposure to the same set of 12 VOCs used in this work. Briefly, the classification model is trained with features extracted from the cycles' curves. Twenty-four features were initially chosen, defined to describe the typical morphology of these curves. For example, while the derivatives describe slow or fast signal rising or decreasing moments, the amplitudes and the area under the curve describe the intensity of the signal. The full description of the extracted features can be found in our previous work.[37] In order to select the best of the twenty-four extracted features, recursive feature elimination with with 10-fold cross validation was used, resulting in the final set of 12 features. The SVM classifier parameters were also tuned, resulting in a radial basis function kernel and parameters $C$: 100 and $\gamma$: 0.1.[37]

In this work, the cycles collected for each hybrid gel formulation were divided into training and testing sets. There was no validation set, as the classification model had been previously validated with independent data of the same type as explained above .[37] Two-thirds of the cycles were used to train the classifier and one-third was used to test it and generate the confusion matrices. There were 606 cycles for the 5CB data set (roughly 49 cycles per VOC), 703 cycles for the


https://doi.org/10.1021/acsami.1c24721
ACS Appl. Mater. Interfaces 2022, 14, 6261−6273

6CB data set (roughly 58 cycles per VOC), 630 cycles for the 7CB data set (roughly 52 cycles per VOC), and 444 cycles for the 8CB formulation (roughly 37 cycles per VOC).

## ■ ASSOCIATED CONTENT

### Supporting Information

The Supporting Information is available free of charge at https://pubs.acs.org/doi/10.1021/acsami.1c24721.

Droplet diameter distribution plots, POM hydrogels, AFM hybrid gels and hydrogels, hybrid gel stability upon storage, POM heating 8CB gels, POM temperature hybrid/control gels, DSC scans, ATR−FTIR plots, Raman spectroscopy, POM and e-nose observations, confusion matrices, accuracy plots control gels, accuracy plot hybrid gels with 6CB 25 s exposure, 6CB 25 s signal exposure example plots, and raw signal data for hybrid/control gels (PDF)

5CB hybrid gel toluene exposure with polarizers at 45 °C (MP4)

8CB hybrid gel ethanol exposure with crossed polarizers (MP4)

## ■ AUTHOR INFORMATION


### Corresponding Author

**Ana Cecília A. Roque** − *Associate Laboratory i4HB—Institute for Health and Bioeconomy, School of Science and Technology and UCIBIO—Applied Molecular Biosciences Unit, Department of Chemistry, School of Science and Technology, NOVA University Lisbon, 2829-516 Caparica, Portugal;* orcid.org/0000-0002-4586-3024; Email: cecilia.roque@fct.unl.pt

### Authors

**Efthymia Ramou** − *Associate Laboratory i4HB—Institute for Health and Bioeconomy, School of Science and Technology and UCIBIO—Applied Molecular Biosciences Unit, Department of Chemistry, School of Science and Technology, NOVA University Lisbon, 2829-516 Caparica, Portugal*

**Susana I. C. J. Palma** − *Associate Laboratory i4HB—Institute for Health and Bioeconomy, School of Science and Technology and UCIBIO—Applied Molecular Biosciences Unit, Department of Chemistry, School of Science and Technology, NOVA University Lisbon, 2829-516 Caparica, Portugal*

Complete contact information is available at: https://pubs.acs.org/10.1021/acsami.1c24721


### Author Contributions

The manuscript was written through contributions of all authors. All authors have given approval to the final version of the manuscript.

### Notes

The authors declare no competing financial interest.

## ■ ACKNOWLEDGMENTS

This project has received funding from the European Research Council (ERC) under the EU Horizon 2020 research and innovation programme (SCENT-ERC-2014-STG-639123, 2015−2022) and by national funds from FCT—Fundação para a Ciência e a Tecnologia, I.P., in the scope of the project PTDC/BII-BIO/28878/2017, UIDP/04378/2020 and UIDB/04378/2020 of the Research Unit on Applied Molecular Biosciences—UCIBIO and the project LA/P/0140/2020 of the Associate Laboratory Institute for Health and Bioeconomy—i4HB. The authors would also like to thank Tomás Calmeiro from CENIMAT|i3N for the AFM images, Ana Marques and Isabel Ferreira from the Energy Materials (EM) Lab for AFM and Raman, and Carla Rodrigues from LAQV analysis lab for the DSC experiments. The authors acknowledge support from previous lab members, namely, Gonçalo Santos, Cláudia Alves, and Fábio Leite.

## ■ REFERENCES


(1) Bisoyi, H. K.; Kumar, S. Liquid-Crystal Nanoscience: An Emerging Avenue of Soft Self-Assembly. *Chem. Soc. Rev.* **2011**, *40*, 306−319.

(2) Esteves, C.; Ramou, E.; Porteira, A. R. P.; Moura Barbosa, A. J.; Roque, A. C. A. Seeing the Unseen: The Role of Liquid Crystals in Gas-Sensing Technologies. *Adv. Opt. Mater.* **2020**, *8*, 1902117.

(3) Ding, X.; Yang, K.-L. Liquid Crystal Based Optical Sensor for Detection of Vaporous Butylamine in Air. *Sens. Actuators, B* **2012**, *173*, 607−613.

(4) Szilvási, T.; Bao, N.; Nayani, K.; Yu, H.; Rai, P.; Twieg, R. J.; Mavrikakis, M.; Abbott, N. L. Redox-Triggered Orientational Responses of Liquid Crystals to Chlorine Gas. *Angew. Chem., Int. Ed.* **2018**, *57*, 9665−9669.

(5) Bi, X.; Yang, K.-L. Real-Time Liquid Crystal-Based Glutaraldehyde Sensor. *Sens. Actuators, B* **2008**, *134*, 432−437.

(6) Esteves, C.; Santos, G. M. C.; Alves, C.; Palma, S. I. C. J.; Porteira, A. R.; Filho, J.; Costa, H. M. A.; Alves, V. D.; Morais Faustino, B. M.; Ferreira, I.; Gamboa, H.; Roque, A. C. A. Effect of Film Thickness in Gelatin Hybrid Gels for Artificial Olfaction. *Mater. Today Bio* **2019**, *1*, 100002.

(7) Hussain, A.; Semeano, A. T. S.; Palma, S. I. C. J.; Pina, A. S.; Almeida, J.; Medrado, B. F.; Pádua, A. C. C. S.; Carvalho, A. L.; Dionísio, M.; Li, R. W. C.; Gamboa, H.; Ulijn, R. V.; Gruber, J.; Roque, A. C. A. Tunable Gas Sensing Gels by Cooperative Assembly. *Adv. Funct. Mater.* **2017**, *27*, 1700803.

(8) Bolleddu, R.; Chakraborty, S.; Bhattacharjee, M.; Bhandaru, N.; Thakur, S.; Gooh-Pattader, P. S.; Mukherjee, R.; Bandyopadhyay, D. Pattern-Directed Phase Transitions and VOC Sensing of Liquid Crystal Films. *Ind. Eng. Chem. Res.* **2020**, *59*, 1902−1913.

(9) Reyes, C. G.; Sharma, A.; Lagerwall, J. P. F. Non-Electronic Gas Sensors from Electrospun Mats of Liquid Crystal Core Fibres for Detecting Volatile Organic Compounds at Room Temperature. *Liq. Cryst.* **2016**, *43*, 1986−2001.

(10) Nayani, K.; Yang, Y.; Yu, H.; Jani, P.; Mavrikakis, M.; Abbott, N. Areas of Opportunity Related to Design of Chemical and Biological Sensors Based on Liquid Crystals. *Liq. Cryst. Today* **2020**, *29*, 24−35.

(11) Nayani, K.; Rai, P.; Bao, N.; Yu, H.; Mavrikakis, M.; Twieg, R. J.; Abbott, N. L. Liquid Crystals with Interfacial Ordering That Enhances Responsiveness to Chemical Targets. *Adv. Mater.* **2018**, *30*, 1706707.

(12) Hu, Q.-Z.; Jang, C.-H. Spontaneous Formation of Micrometer-Scale Liquid Crystal Droplet Patterns on Solid Surfaces and Their Sensing Applications. *Soft Matter* **2013**, *9*, 5779−5784.

(13) Lai, Y.-T.; Kuo, J.-C.; Yang, Y.-J. A Novel Gas Sensor Using Polymer-Dispersed Liquid Crystal Doped with Carbon Nanotubes. *Sens. Actuators, A* **2014**, *215*, 83−88.

(14) Wang, J.; Jákli, A.; West, J. L. Liquid Crystal/Polymer Fiber Mats as Sensitive Chemical Sensors. *J. Mol. Liq.* **2018**, *267*, 490−495.

(15) Li, Y.; Chen, Y.; Yi, D.; Du, Y.; Luo, W.; Hong, X.; Li, X.; Geng, Y.; Luo, D. A Self-Assembled Fiber Mach-Zehnder Interferometer Based on Liquid Crystals. *J. Mater. Chem. C* **2020**, *8*, 11153−11159.

(16) Semeano, A. T. S.; Maffei, D. F.; Palma, S.; Li, R. W. C.; Franco, B. D. G. M.; Roque, A. C. A.; Gruber, J. Tilapia Fish Microbial Spoilage Monitored by a Single Optical Gas Sensor. *Food Control* **2018**, *89*, 72−76.

(17) Drzaic, P. S. Nematic Configurations Within Droplets. In *Liquid Crystal Dispersions*; World Scientific: Singapore, 1995; pp 99–181.
(18) Lavrentovich, O. D.; Pergamenshchik, V. M. Patterns in Thin Liquid Crystal Films and the Divergence (Surfacelike) Elasticity. *Int. J. Mod. Phys. B* **1995**, *9*, 2389–2437.
(19) Kleman, M.; Lavrentovich, O. D. *Soft Matter Physics: An Introduction. Partially Ordered Systems*; Springer-Verlag: New York, 2003.
(20) Kim, Y. H.; Yoon, D. K.; Choi, M. C.; Jeong, H. S.; Kim, M. W.; Lavrentovich, O. D.; Jung, H.-T. Confined Self-Assembly of Toric Focal Conic Domains (The Effects of Confined Geometry on the Feature Size of Toric Focal Conic Domains). *Langmuir* **2009**, *25*, 1685–1691.
(21) Kim, Y. H.; Lee, J.-O.; Jeong, H. S.; Kim, J. H.; Yoon, E. K.; Yoon, D. K.; Yoon, J.-B.; Jung, H.-T. Optically Selective Microlens Photomasks Using Self-Assembled Smectic Liquid Crystal Defect Arrays. *Adv. Mater.* **2010**, *22*, 2416–2420.
(22) Designolle, V.; Herminghaus, S.; Pfohl, T.; Bahr, C. AFM Study of Defect-Induced Depressions of the Smectic-A/Air Interface. *Langmuir* **2006**, *22*, 363–368.
(23) Popov, P.; Mann, E. K.; Jákli, A. Thermotropic Liquid Crystal Films for Biosensors and Beyond. *J. Mater. Chem. B* **2017**, *5*, 5061–5078.
(24) Cumberland, J.; Lopatkina, T.; Murachver, M.; Popov, P.; Kenderesi, V.; Buka, Á.; Mann, E. K.; Jákli, A. Bending Nematic Liquid Crystal Membranes with Phospholipids. *Soft Matter* **2018**, *14*, 7003–7008.
(25) Vorländer, D. Über Die Natur Der Kohlenstoffketten in Kristallin-Flüssigen Substanzen. *Z. Phys. Chem.* **1927**, *126*, 449.
(26) Griffin, A. C.; Britt, T. R. Effect of Molecular Structure on Mesopmorphisim. Flexible-Center Siamese-Twin Liquid Crystalline Diesters- A "Prepolymer" Model. *J. Am. Chem. Soc.* **1981**, *103*, 4957–4959.
(27) Dunmur, D. A.; Miller, W. H. Volumetric Studies of the Homologous Series of Alkyl-Cyano-Biphenyl Liquid Crystals. *J. Phys., Colloq.* **1979**, *40*, C3-141–C3-146.
(28) Hakemi, H.; Jagodzinski, E. F.; DuPré, D. B. The Determination of the Elastic Constants of a Series of N-Alkylcyanobiphenyls by Anisotropy of Turbidity. *J. Chem. Phys.* **1983**, *78*, 1513–1518.
(29) Dwivedi, M. K.; Tiwari, S. N. Odd-Even Effect in p-Alkyl-P′-Cyanobiphenyl Liquid Crystalline Series: An Ab Initio Study. *J. Mol. Liq.* **2011**, *158*, 208–211.
(30) Kitzerow, H.-S. Polymer-Dispersed Liquid Crystals From the Nematic Curvilinear Aligned Phase to Ferroelectric Films. *Liq. Cryst.* **1994**, *16*, 1–31.
(31) Radian-Guenebaud, M.; Sixou, P. Droplet Size Effects in Polymer Dispersed Nematic Chiral Liquid Crystal Materials. *Mol. Cryst. Liq. Cryst. Sci. Technol., Sect. A* **1992**, *220*, 53–62.
(32) Shanks, R. A.; Staszczyk, D. Thermal and Optical Characterization of Polymer-Dispersed Liquid Crystals. *Int. J. Polym. Sci.* **2012**, *2012*, 767581.
(33) Liang, H.-L.; Zentel, R.; Rudquist, P.; Lagerwall, J. Towards Tunable Defect Arrangements in Smectic Liquid Crystal Shells Utilizing the Nematic-Smectic Transition in Hybrid-Aligned Geometries. *Soft Matter* **2012**, *8*, 5443–5450.
(34) Cladis, P. E.; Torza, S. Growth of a Smectic A from a Bent Nematic Phase and the Smectic Light Valve. *J. Appl. Phys.* **1975**, *46*, 584–599.
(35) Rodrigues, R.; Palma, S. I. C. J.; Correia, V. G.; Padrão, I.; Pais, J.; Banza, M.; Alves, C.; Deuermeier, J.; Martins, C.; Costa, H. M. A.; Ramou, E.; Silva Pereira, C.; Roque, A. C. A. Sustainable Plant Polyesters as Substrates for Optical Gas Sensors. *Mater. Today Bio* **2020**, *8*, 100083.
(36) Schelski, K.; Reyes, C. G.; Pschyklenk, L.; Kaul, P.-M.; Lagerwall, J. P. F. Quantitative Volatile Organic Compound Sensing with Liquid Crystal Core Fibers. *Cell Rep. Phys. Sci.* **2021**, *2*, 100661.
(37) Santos, G.; Alves, C.; Pádua, A. C.; Palma, S.; Gamboa, H.; Roque, A. C. An Optimized E-Nose for Efficient Volatile Sensing and Discrimination. In *Proceedings of the 12th International Joint Conference on Biomedical Engineering Systems and Technologies-Volume 1 BIODEVICES: BIODEVICES*; Roque, A., Fred, A., Gamboa, H., Eds.; SCITEPRESS: Prague, Czech Republic, 2019; pp 36–46.




https://doi.org/10.1021/acsami.1c24721
*ACS Appl. Mater. Interfaces* 2022, 14, 6261–6273